Interaction and Multiscale Mechanics, Vol. 2, No. 4 (2009) 413-430
DOI: http://dx.doi.org/10.12989/imm.2009.2.4.413

Displacements of the helical stator tooth for an electromechanical integrated toroidal drive

Lizhong Xu† and Dazhou Zheng

Mechanical engineering institute, Yanshan University, Qinhuangdao 066004, China

(Received August 22, 2009, Accepted October 28, 2009)

Abstract. The stator tooth is a key component of the electromechanical integrated toroidal drive system. The stator tooth is spiral in shape and the calculation of its displacements is difficult. In this paper, using the coordinate transformation method, the displacements of the stator tooth in the local coordinate system are expressed as the function of the variable in the drive coordinate system. Using the minimum potential energy principle, the equations of the displacements of the stator tooth under the loads are deduced. The displacement distributions within the stator tooth are investigated and the changes of the displacement distributions along with the main parameters are analyzed. This research can offer the basis for the strength and stiffness design of the drive system.

Keywords: toroidal drive; electromechanical integrated; displacement; strain energy.

1. Introduction

A toroidal drive can transmit large torques in a very small size and is suitable for applications to the technical fields such as aviation and space flight, etc (Kuehnle *et al*. 1981, Yao *et al*. 2006, Wei *et al*. 2008). As more and more electrical and control techniques are utilized in the mechanical engineering field, electromechanical integrated drive systems have become an advancing edge of the mechanical science.

Many types of the magnetic gear drive have been proposed and investigated recently (Mezani *et al*. 2006, Jorgensen *et al*. 2008, Wang *et al*. 2006, Liu *et al*. 2009). The magnetic gear drives are passive drive systems in which meshing occurs without physical contact. The electromagnetic harmonic drive (Delin and Huamin 1993) and piezoelectric harmonic drive (Oliver 2000) are active drive systems in which the meshing forces between the flexible and rigid gears are controlled by the electromagnetic or piezoelectric force with the drive and power integrated.

Based on the toroidal drive (Xu and Huang 2003), the authors presented a kind of electromechanical integrated drive system without contact, i.e., the electromechanical integrated toroidal drive. This drive is a new concept of the generalized composite drive. With this drive, the toroidal drive, power and control are all integrated (Xu and Huang 2005). The drive consists of four basic elements as shown in Fig. 1: (a) radically positioned planets; (b) a central worm; (c) a toroidal shaped stator; and (d) a rotor, which forms the central output shaft upon which the planets are

† Professor, Corresponding author, E-mail: Xlz@ysu.edu.cn

mounted. The central worm is fixed and the coils are mounted along the helical grooves of its surface. The planets have permanent magnets instead of teeth. The *N* and *S* polar permanent magnets are mounted alternately on a planet. Te stator has helical permanent magnets instead of helical teeth. In the same manner as the planet, the *N* and *S* polar helical permanent magnets are mounted alternately on the stator. Besides permanent magnets, steel plates can also be used for the teeth of the stator. When the teeth of the stator are produced with plate permanent magnets, the plate permanent magnet has also two poles. The pole axis of the magnet is perpendicular to the plate permanent magnet surface. One pole is near the planet and the other pole is located on the other surface of the magnet plate. As the teeth of the planet are also permanent magnets, between the planet teeth and steel plate, enough magnetic force can be generated as well. Therefore, under the condition that the torque to be transmitted is not large, the teeth of the stator can be produced with steel plates as well. Cylinder or segment permanent magnets can be used for the teeth of the planet. The cylinder or segment permanent magnets are mounted on the planet body by bonding or other joints. The central worm consists of a number of silicon steel sheets. Several helical slots are cut on the worm. The windings made of insulated wires are mounted along the helical slots.

If the relation between the planet pitch, tooth number and helical angle on the stator, and number of pole pairs and helical angle on the worm is specified, then the *N* pole of one element will correspond to the *S* pole of the other element all along. The attractive forces between the *N* and *S* poles of the different elements are the driving forces and meshing occurs without physical contact. When the alternate current is charged into the coils of the worm, a toroidal circular field is formed. It can drive several planets rotating about their own axis. And by means of magnetic forces between the teeth of the planet and stator, the rotor is driven to rotate about its own axis. Thus, a power of low speed and large torque is generated.

Compared with the toroidal drive, the new drive can be easily produced, without wear, and with no need for lubrication. It can be substituted for a servo system to simplify the structure of the existing electromechanical systems. Besides the above-mentioned fields that require compactness, the drive can be used in fields that require accurate control, such as robots, etc.

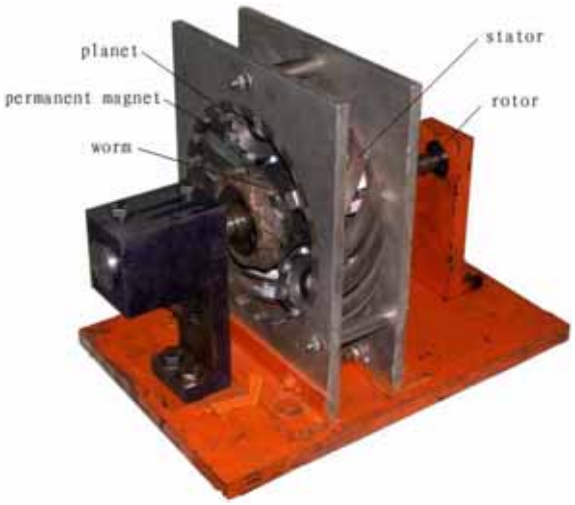

Fig. 1 The model machine for the drive system

The authors have conducted some research for the drive system to investigate the driving torque and its affecting factors (Xu and Huang 2005), while presenting a control theory for the drive system (Xu and Fan 2006). As the loading torque becomes large, one should pay special attention to the strength and stiffness problems of the drive system. The stator tooth is the key component of the drive system, of which the strength and stiffness have important influence on the operating performance of the drive system. When the drive is in operation, speed fluctuation can occur with the output shaft. It is mainly caused by the non-uniform air-gap between the stator teeth and the planet teeth, which can be attributed to two factors. One is the manufacturing and mounting errors of the machine, another is the elastic displacements of the stator teeth. When the manufacturing and mounting errors are ignored, an elastic displacement of 0.04 mm for the stator tooth can cause a speed fluctuation of about 8% for the output shaft under the condition that the air-gap between the stator teeth and the planet teeth is about 0.5 mm. To reduce the speed fluctuation, the manufacturing and mounting accuracy should be improved. Besides this, the stiffness of the stator teeth should be chosen properly. Therefore, it becomes a prerequisite to calculate the elastic displacement analysis of the stator teeth, which serves as the basis for designing the stiffness of the stator teeth. The problem can be resolved using standard finite elements codes. However, an analytical solution has one obvious advantage over the finite element solution, because it enables us to draw some inherent rules that are favorable for the parameter design and optimum of the drive system. For the reason stated, we shall focus on derivation of an analytical solution for the stator tooth that is spiral in shape.

In this paper, the coordinate systems for the drive system and its stator tooth are established, and the transformation matrices between the different coordinate systems are presented. Based on this, the displacements of the stator tooth in the local coordinate system are expressed as a function of the variables in the drive coordinate system. Using the minimum potential energy principle and selecting proper trial function, the equations of the displacements of the stator tooth under the loads arederived. Using these equations, the displacement distributions within the stator tooth for the drive system are investigated and the changes of the displacement distributions with respect to the main parameters are analyzed. The results show that the related parameters have obvious influence on the displacement distribution of the stator tooth. In order to decrease the displacements of the stator tooth, these parameters should be selected properly. The present research offers a useful basis for the strength and stiffness design of the drive system.

2. Coordinate transformation

Fig. 2 shows a helical stator tooth and its related coordinate systems. As the stator teeth are all of helical surface, their displacement calculation is quite complicated. In order to obtain the displacement, we must use the coordinate transformation principles. To this end, we select the coordinate systems for electromechanical integrated toroidal drive as shown in Fig. 2. The coordinate system $s\,(x, y, z)$ is attached to the stator, $s_1\,(x_1, y_1, z_1)$ is attached to the planet, $s_2\,(x_2, y_2, z_2)$ to the normal section of the stator tooth, $s_r\,(x_r, y_r, z_r)$ to the rotor, and $s_{10}\,(x_{10}, y_{10}, z_{10})$ also to the rotor. The z_2- and z_r-axes are the rotating axes of the rotor, particularly the z_1-axis is the rotating axis of the planet. Here, ϕ_1 is the planet rotating angle, R is the planet radius, λ is the lead angle of the stator tooth, $\tan\lambda = \dfrac{z_s R}{z_1(a + R\cos\phi_1)}$, with a indicating the central distance between the planet and

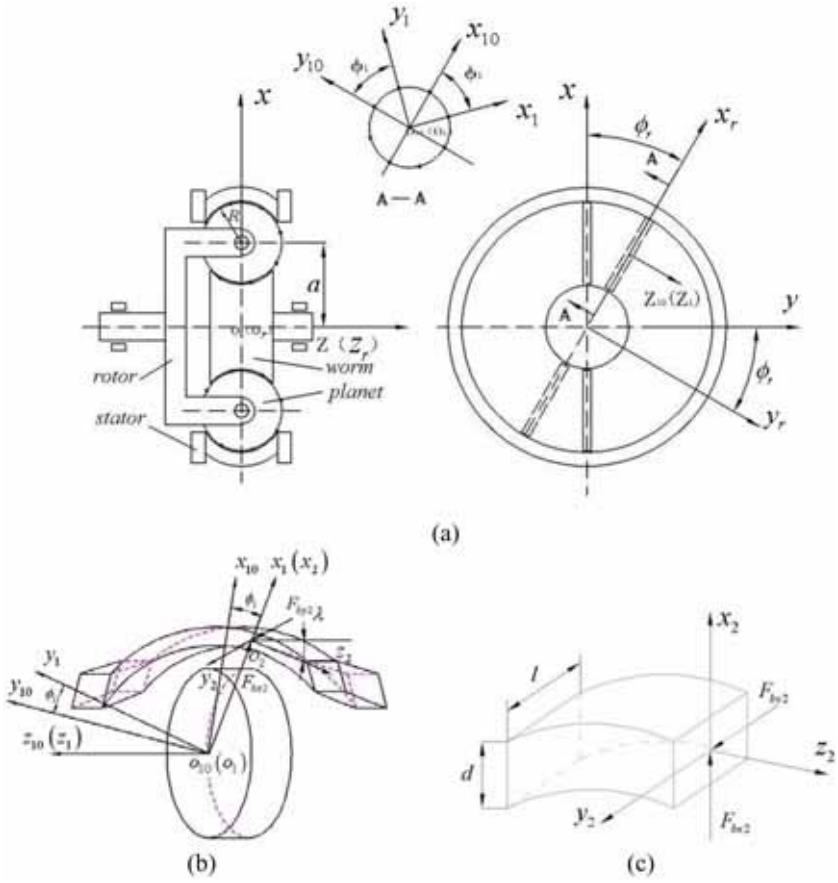

Fig. 2 The coordinate systems for the drive and its stator tooth (a) Coordinate systems of the drive, (b) Coordinate systems of the planet and a stator tooth, (c) Coordinate system on the cross section of a stator tooth

stator, z_s is the tooth number of the stator, and z_1 is the tooth number of the planet.

The matrices $\boldsymbol{M}_{101}$, $\boldsymbol{M}_{r10}$, $\boldsymbol{M}_{0r}$ and $\boldsymbol{M}_{21}$ are the coordinates transformation matrices from the coordinate system s_{10} to the system s_1, from the system s_{10} to the system s_r, from the system s_r to the system s, and from the system s_1 to the system s_2, respectively. These matrices can be given as follows:

$$\boldsymbol{M}_{101} = \begin{bmatrix} \cos\phi_1 & \sin\phi_1 & 0 \\ -\sin\phi_1 & \cos\phi_1 & 0 \\ 0 & 0 & 1 \end{bmatrix} \tag{1}$$

$$\boldsymbol{M}_{r10} = \begin{bmatrix} 1 & 0 & 0 & a \\ 0 & 0 & 1 & 0 \\ 0 & -1 & 0 & 0 \\ 0 & 0 & 0 & 1 \end{bmatrix} \tag{2}$$

$$\boldsymbol{M}_{0r} = \begin{bmatrix} \cos\phi_r & -\sin\phi_r & 0 \\ \sin\phi_r & \cos\phi_r & 0 \\ 0 & 0 & 1 \end{bmatrix} \tag{3}$$

$$\boldsymbol{M}_{21} = \begin{bmatrix} 1 & 0 & 0 & -R \\ 0 & \cos\lambda & \sin\lambda & 0 \\ 0 & -\sin\lambda & \cos\lambda & 0 \\ 0 & 0 & 0 & 1 \end{bmatrix} \tag{4}$$

3. The minimum potential energy principle and the displacement function

In order to obtain the displacement of the helical stator tooth, we use the minimum potential energy principle as below:

$$\delta E_t = 0 \tag{5}$$

where $E_t = U - W$, U is the strain energy of the stator tooth, and W is the work of the forces. From Eq. (5), one obtains

$$\delta U = \delta W \tag{6}$$

where δU and δW are the virtual strain energy and virtual work, respectively.

The virtual strain energy of the stator tooth can be given as follows:

$$\delta U = \frac{1}{2}\iiint(\sigma_{x2}\delta\varepsilon_{x2} + \sigma_{y2}\delta\varepsilon_{y2} + \sigma_{z2}\delta\varepsilon_{z2} + \tau_{x2y2}\delta\gamma_{x2y2} + \tau_{y2z2}\delta\gamma_{y2z2} + \tau_{z2x2}\delta\gamma_{z2x2})dV \tag{7}$$

where $\sigma_{x2}, \sigma_{y2}, \sigma_{z2}$ are the stress components of the stator tooth in the coordinate axes x_2, y_2 and z_2, respectively; $\varepsilon_{x2}, \varepsilon_{y2}, \varepsilon_{z2}$, are the strain components of the stator tooth in the coordinate axes x_2, y_2 and z_2, respectively; $\tau_{x2y2}, \tau_{y2z2}, \tau_{z2x2}$ are the shear stress components of the stator tooth in three different directions, respectively; $\gamma_{x2y2}, \gamma_{y2z2}, \gamma_{z2x2}$ are the shear strain components of the stator tooth in three different directions, respectively; and V is the volume of the stator tooth.

The virtual work done by the loads applied to the stator tooth can be given as follows:

$$\delta W = \iiint_V (F_{bx2}\delta u_2 + F_{by2}\delta v_2 + F_{bz2}\delta w_2)dV \tag{8}$$

where F_{bi} is the load applied to the stator tooth ($i = x_2$, y_2 and z_2), u_2, v_2 and w_2 are the displacements of the stator tooth in the coordinate axes x_2, y_2 and z_2, respectively.

Eq. (7) can be changed into the following form

$$\delta U = \int_0^L (\delta\varepsilon_{x_2}T_{x_2} + \delta\varepsilon_{y_2}T_{y_2} + \delta\varepsilon_{z_2}N_2 + \delta\gamma_{x_2z_2}F_{x_2} + \delta\gamma_{y_2z_2}F_{y_2} + \delta\gamma_{x_2y_2}T_2)ds \tag{9a}$$

where T_{x_2} is the bending moment about axis x_2, T_{y_2} the bending moment about axis y_2, N_2 is the tension force in the z_2 direction, F_{x_2} is the shear force in the x_2 direction, F_{y_2} is the shear force in the y_2 direction, and T_2 is the torsional moment about axis z_2,

$$T_{x_2} = \int_A y_2 \sigma_{z_2} dA = EI_{x_2} \varepsilon_{x_2}, T_{y_2} = \int_A x_2 \sigma_{z_2} dA = EI_{y_2} \varepsilon_{y_2}, N_2 = \int_A \sigma_{z_2} dA = EA\varepsilon_{z_2}, F_{x_2} = \int_A \tau_{x_2 z_2} dA = k_{x_2} GA\gamma_{x_2 z_2}$$

$$F_{y_2} = \int_A \tau_{y_2 z_2} dA = k_{y_2} GA\gamma_{y_2 z_2}, T_2 = \int_A (x_2 \tau_{y_2 z_2} - y_2 \tau_{x_2 z_2}) dA = k_{x_2} GJ\gamma_{x_2 z_2} \tag{9b}$$

Here, A is the transverse cross-sectional area of the stator tooth, E is the modulus of elasticity of the stator tooth material, G is its shear modulus of elasticity, I_{x2} is the second moments of area of the tooth about axis x_2 ($I_{x2} = dl^3 / 12$, where l and d are the width and thickness of the tooth, respectively), and I_{y2} is the second moments of area of the tooth about axis y_2 ($I_{y2} = ld^3 / 12$).

To simplify the analysis, the strain components of the stator tooth in the coordinate system s_2 can be expressed in terms of the strain components in the coordinate system s, that is,

$$\begin{bmatrix} \varepsilon_{x_2} \\ \varepsilon_{y_2} \\ \varepsilon_{z_2} \\ \gamma_{x_2 y_2} \\ \gamma_{y_2 z_2} \\ \gamma_{x_2 z_2} \end{bmatrix} = \begin{bmatrix} l_1^2 & m_1^2 & n_1^2 & l_1 m_1 & m_1 n_1 & n_1 l_1 \\ l_2^2 & m_2^2 & n_2^2 & l_2 m_2 & m_2 n_2 & n_2 l_2 \\ l_3^2 & m_3^2 & n_3^2 & l_3 m_3 & m_3 n_3 & n_3 l_3 \\ 2l_1 l_2 & 2m_1 m_2 & 2n_1 n_2 & l_1 m_2 + l_2 m_1 & m_1 n_2 + m_2 n_1 & n_1 l_2 + n_2 l_1 \\ 2l_2 l_3 & 2m_2 m_3 & 2n_2 n_3 & l_2 m_3 + l_3 m_2 & m_2 n_3 + m_3 n_2 & n_2 l_3 + n_3 l_2 \\ 2l_3 l_1 & 2m_3 m_1 & 2n_3 n_1 & l_3 m_1 + l_1 m_3 & m_3 n_1 + m_1 n_3 & n_3 l_1 + n_1 l_3 \end{bmatrix} \begin{bmatrix} \varepsilon_x \\ \varepsilon_y \\ \varepsilon_z \\ \gamma_{xy} \\ \gamma_{yz} \\ \gamma_{xz} \end{bmatrix} \tag{10a}$$

where

$$\begin{bmatrix} l_1 & m_1 & n_1 \\ l_2 & m_2 & n_2 \\ l_3 & m_3 & n_3 \end{bmatrix} = \begin{bmatrix} \cos\phi_1 \cos\phi_r & \cos\phi_1 \sin\phi_r & \sin\phi_1 \\ \cos\lambda \sin\phi_1 \cos\phi_r - \sin\lambda \sin\phi_r & \cos\lambda \sin\phi_1 \sin\phi_r + \sin\lambda \cos\phi_r & -\cos\lambda \cos\phi_1 \\ -\sin\lambda \sin\phi_1 \cos\phi_r - \cos\lambda \sin\phi_r & -\sin\lambda \sin\phi_1 \sin\phi_r + \cos\lambda \cos\phi_r & \sin\lambda \cos\phi_1 \end{bmatrix} \tag{10b}$$

The strains of the tooth can be expressed as functions of the displacements,

$$\varepsilon_x = \frac{\partial u}{\partial x} = \frac{\partial u}{\partial \phi_1} \frac{\partial \phi_1}{\partial x} \tag{11a}$$

$$\varepsilon_y = \frac{\partial v}{\partial y} = \frac{\partial v}{\partial \phi_1} \frac{\partial \phi_1}{\partial y} \tag{11b}$$

$$\varepsilon_z = \frac{\partial w}{\partial z} = \frac{\partial w}{\partial \phi_1} \frac{\partial \phi_1}{\partial z} \tag{11c}$$

$$\gamma_{xy} = \frac{\partial u}{\partial y} + \frac{\partial v}{\partial x} = \frac{\partial u}{\partial \phi_1} \frac{\partial \phi_1}{\partial y} + \frac{\partial v}{\partial \phi_1} \frac{\partial \phi_1}{\partial x} \tag{11d}$$

$$\gamma_{yz} = \frac{\partial v}{\partial z} + \frac{\partial w}{\partial y} = \frac{\partial v}{\partial \phi_1} \frac{\partial \phi_1}{\partial z} + \frac{\partial w}{\partial \phi_1} \frac{\partial \phi_1}{\partial y} \tag{11e}$$

$$\gamma_{zx} = \frac{\partial w}{\partial x} + \frac{\partial u}{\partial z} = \frac{\partial w}{\partial \phi_1} \frac{\partial \phi_1}{\partial x} + \frac{\partial u}{\partial \phi_1} \frac{\partial \phi_1}{\partial z} \tag{11f}$$

In coordinate system $s_{10}(x_{10}, y_{10}, z_{10})$, a point on the stator tooth can be expressed as

$$\begin{cases} x_{10} = R\cos\phi_1 \\ y_{10} = -R\sin\phi_1 \\ z_{10} = 0 \end{cases} \tag{12}$$

Using the coordinates transformation, the point can be given in the coordinate system $s(x, y, z)$ as follows:

$$\begin{bmatrix} x \\ y \\ z \\ 1 \end{bmatrix} = \boldsymbol{M}_{0r}\boldsymbol{M}_{r10}\begin{bmatrix} x_{10} \\ y_{10} \\ z_{10} \\ 1 \end{bmatrix} = \begin{bmatrix} (R\cos\phi_1 + a)\cos\phi_r \\ (R\cos\phi_1 + a)\sin\phi_r \\ R\sin\phi_1 \\ 1 \end{bmatrix} \tag{13}$$

From Eq. (13), $\frac{\partial\phi_1}{\partial x}$, $\frac{\partial\phi_1}{\partial y}$ and $\frac{\partial\phi_1}{\partial z}$ can be obtained as follows:

$$\phi_x = \frac{\partial\phi_1}{\partial x} = \frac{1}{-R\left(\sin\phi_1\cos\frac{z_1\phi_1}{z_s} + \frac{z_1}{z_s}\cos\phi_1\sin\frac{z_1\phi_1}{z_s} + \frac{z_1 a}{z_s R}\sin\frac{z_1\phi_1}{z_s}\right)} \tag{14a}$$

$$\phi_y = \frac{\partial\phi_1}{\partial y} = \frac{1}{-R\left(\sin\phi_1\sin\frac{z_1\phi_1}{z_s} - \frac{z_1}{z_s}\cos\phi_1\cos\frac{z_1\phi_1}{z_s} - \frac{z_1 a}{z_s R}\cos\frac{z_1\phi_1}{z_s}\right)} \tag{14b}$$

$$\phi_z = \frac{\partial\phi_1}{\partial z} = \frac{1}{R\cos\phi_1} \tag{14c}$$

Let the trial function of the displacements u, v and w be as follows:

$$u(\phi_1) = a_1\sin\frac{\pi(\phi_1 - \theta_1)}{\Delta\theta} + a_2\sin\frac{2\pi(\phi_1 - \theta_1)}{\Delta\theta} + \ldots + a_n\sin\frac{n\pi(\phi_1 - \theta_1)}{\Delta\theta} + \ldots = \sum_{n=1}^{\infty} a_n\sin\frac{n\pi(\phi_1 - \theta_1)}{\Delta\theta} \tag{15a}$$

$$v(\phi_1) = b_1\sin\frac{\pi(\phi_1 - \theta_1)}{\Delta\theta} + b_2\sin\frac{2\pi(\phi_1 - \theta_1)}{\Delta\theta_1} + \ldots + b_n\sin\frac{n\pi(\phi_1 - \theta_1)}{\Delta\theta} + \ldots = \sum_{n=1}^{\infty} b_n\sin\frac{n\pi(\phi_1 - \theta_1)}{\Delta\theta} \tag{15b}$$

$$w(\phi_1) = c_1\sin\frac{\pi(\phi_1 - \theta_1)}{\Delta\theta} + c_2\sin\frac{2\pi(\phi_1 - \theta_1)}{\Delta\theta} + \ldots + c_n\sin\frac{n\pi(\phi_1 - \theta_1)}{\Delta\theta} + \ldots = \sum_{n=1}^{\infty} c_n\sin\frac{n\pi(\phi_1 - \theta_1)}{\Delta\theta} \tag{15c}$$

where $\Delta\theta = \theta_2 - \theta_1$, θ_1, and θ_2 are the initial and end mesh angles of the planet tooth as shown in Fig. 3. From Eq. (15), $\frac{\partial u}{\partial\phi_1}$, $\frac{\partial v}{\partial\phi_1}$ and $\frac{\partial w}{\partial\phi_1}$ can be calculated.

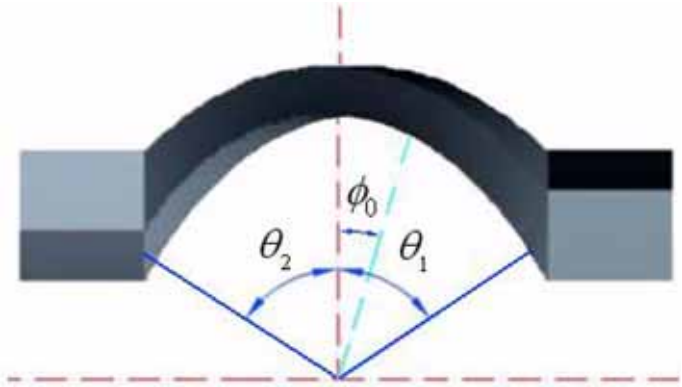

Fig. 3 The initial and end angles of the planet tooth meshing with the stator tooth

In the coordinate system $s(x, y, z)$, the arc length ds can be calculated using Eqs. (13) and (15),

$$ds = \sqrt{(x'^2 + y'^2 + z'^2)}d\phi_1 = RSd\phi_1 \tag{16a}$$

where

$$S = \sqrt{\left(\frac{z_1}{z_s}\sin\frac{z_1\phi}{z_s}\cos\phi_1 + \cos\frac{z_1\phi}{z_s}\sin\phi_1 + \frac{z_1 a}{z_s R}\sin\frac{z_1\phi}{z_s}\right)^2 + \left(\frac{z_1}{z_s}\cos\frac{z_1\phi}{z_s}\cos\phi_1 - \sin\frac{z_1\phi}{z_s}\sin\phi_1 + \frac{z_1 a}{z_s R}\cos\frac{z_1\phi}{z_s}\right)^2 + (\cos\phi_1)^2} \tag{16b}$$

Combining Eqs. (9) with (10), (11), (14), (15) and (16), the strain energy of the stator tooth can be determined.

If the magnetic forces F_{bx2} and F_{by2} are applied to the stator tooth (see Fig. 2), with the angle of the acting point denoted by ϕ_0, the work done by the forces can be computed from Eq. (8) as

$$W = F_{bx2}u_2(\phi_0) + F_{by2}v_2(\phi_0) \tag{17a}$$

where

$$\begin{bmatrix} u_2 \\ v_2 \\ w_2 \\ 0 \end{bmatrix} = B\begin{bmatrix} u \\ v \\ w \\ 0 \end{bmatrix}, \text{ here } B = M_{21}M_{110}M_{10r}M_{r0} = \begin{bmatrix} B_{11} & B_{12} & B_{13} & B_{14} \\ B_{21} & B_{22} & B_{23} & B_{24} \\ B_{31} & B_{32} & B_{33} & B_{34} \\ B_{41} & B_{42} & B_{43} & B_{44} \end{bmatrix} \tag{17b}$$

Substituting Eq. (17) and the strain energy of the stator tooth into Eq. (6) yields

$$\begin{cases} \dfrac{\partial U}{\partial a_i} = \dfrac{\partial W}{\partial a_i} \\ \dfrac{\partial U}{\partial b_i} = \dfrac{\partial W}{\partial b_i} \\ \dfrac{\partial U}{\partial c_i} = \dfrac{\partial W}{\partial c_i} \end{cases} \quad (i = 1, 2, ...K) \tag{18}$$

From Eq. (18), one obtains

$$\begin{pmatrix} A_{11} & A_{12} & A_{13} \\ A_{21} & A_{22} & A_{23} \\ A_{31} & A_{32} & A_{33} \end{pmatrix} \begin{pmatrix} a_1 \\ \vdots \\ a_k \\ b_1 \\ \vdots \\ b_k \\ c_1 \\ \vdots \\ c_k \end{pmatrix} = \begin{pmatrix} (F_{bx2}B_{11} + F_{by2}B_{21})\sin\dfrac{\pi(\phi_0 - \theta_1)}{\Delta\theta} \\ \vdots \\ (F_{bx2}B_{11} + F_{by2}B_{21})\sin\dfrac{k\pi(\phi_0 - \theta_1)}{\Delta\theta} \\ (F_{bx2}B_{12} + F_{by2}B_{22})\sin\dfrac{\pi(\phi_0 - \theta_1)}{\Delta\theta} \\ \vdots \\ (F_{bx2}B_{12} + F_{by2}B_{22})\sin\dfrac{k\pi(\phi_0 - \theta_1)}{\Delta\theta} \\ (F_{bx2}B_{13} + F_{by2}B_{23})\sin\dfrac{\pi(\phi_0 - \theta_1)}{\Delta\theta} \\ \vdots \\ (F_{bx2}B_{13} + F_{by2}B_{23})\sin\dfrac{k\pi(\phi_0 - \theta_1)}{\Delta\theta} \end{pmatrix} \tag{19}$$

where $A_{ij} = \begin{bmatrix} a_{11} & \cdots & a_{1k} \\ \vdots & \ddots & \vdots \\ a_{k1} & \cdots & a_{kk} \end{bmatrix}$

In matrix A_{11} :

$$a_{ij} = 2EI_{x_2}\int_{\theta_1}^{\theta_2} C_{ij}(l_1^2\phi_x + l_1m_1\phi_y + n_1l_1\phi_z)^2 Sd\phi_1 S + 2EI_{y_2}\int_{\theta_1}^{\theta_2} C_{ij}(l_2^2\phi_x + l_2m_2\phi_y + n_2l_2\phi_z)^2 Sd\phi_1$$
$$+ 2EA\int_{\theta_1}^{\theta_2} C_{ij}(l_3^2\phi_x + l_3m_3\phi_y + n_3l_3\phi_z)^2 Sd\phi_1 + 2k_{x_2}GA\int_{\theta_1}^{\theta_2} C_{ij}(2l_1l_2\phi_x + (l_1m_2 + l_2m_1)\phi_y + (n_2l_1 + n_1l_2)\phi_z)^2 Sd\phi_1$$
$$+ 2k_{y_2}GA\int_{\theta_1}^{\theta_2} C_{ij}(2l_2l_3\phi_x + (l_2m_3 + l_3m_2)\phi_y + (n_2l_3 + n_3l_2)\phi_z)^2 Sd\phi_1$$
$$+ 2GJ\int_{\theta_1}^{\theta_2} C_{ij}(2l_3l_1\phi_x + (l_3m_1 + l_1m_3)\phi_y + (n_3l_1 + n_1l_3)\phi_z)^2 d\phi_1$$

In matrix A_{12} :

$$a_{ij} = 2EI_{x_2}\int_{\theta_1}^{\theta_2} C_{ij}(m_1^2\phi_y + l_1m_1\phi_x + m_1n_1\phi_z)(l_1^2\phi_x + l_1m_1\phi_y + n_1l_1\phi_z)Sd\phi_1 S$$
$$+ 2EI_{y_2}\int_{\theta_1}^{\theta_2} C_{ij}(m_2^2\phi_y + l_2m_2\phi_x + m_2n_2\phi_z)(l_2^2\phi_x + l_2m_2\phi_y + n_2l_2\phi_z)Sd\phi_1$$
$$+ 2EA\int_{\theta_1}^{\theta_2} C_{ij}(m_3^2\phi_y + l_3m_3\phi_x + m_3n_3\phi_z)(l_3^2\phi_x + l_3m_3\phi_y + n_3l_3\phi_z)Sd\phi_1$$
$$+ 2k_{x_2}GA\int_{\theta_1}^{\theta_2} C_{ij}(2m_1m_2\phi_y + (l_1m_2 + l_2m_1)\phi_x + (m_1n_2 + m_2n_1)\phi_z)$$

$$(2l_1l_2\phi_x+(l_1m_2+l_2m_1)\phi_y+(n_2l_1+n_1l_2)\phi_z)Sd\phi_1$$

$$+2k_{y_2}GA\int_{\theta_1}^{\theta_2}C_{ij}(2m_2m_3\phi_y+(l_2m_3+l_3m_2)\phi_x+(m_2n_3+m_3n_2)\phi_z)$$

$$(2l_2l_3\phi_x+(l_2m_3+l_3m_2)\phi_y+(n_2l_3+n_3l_2)\phi_z)Sd\phi_1$$

$$+2GJ\int_{\theta_1}^{\theta_2}C_{ij}(2m_3m_1\phi_y+(l_3m_1+l_1m_3)\phi_x+(m_3n_1+m_1n_3)\phi_z)(2l_3l_1\phi_x+(l_3m_1+l_1m_3)\phi_y+(n_3l_1+n_1l_3)\phi_z)d\phi_1$$

In matrix A_{13}:

$$a_{ij}=2EI_{x_2}\int_{\theta_1}^{\theta_2}C_{ij}(n_1^2\phi_z+m_1n_1\phi_y+n_1l_1\phi_x)(l_1^2\phi_x+l_1m_1\phi_y+n_1l_1\phi_z)Sd\phi_1S$$

$$+2EI_{y_2}\int_{\theta_1}^{\theta_2}C_{ij}(n_2^2\phi_z+m_2n_2\phi_y+n_2l_2\phi_x)(l_2^2\phi_x+l_2m_2\phi_y+n_2l_2\phi_z)Sd\phi_1$$

$$+2EA\int_{\theta_1}^{\theta_2}C_{ij}(n_3^2\phi_z+m_3n_3\phi_y+n_3l_3\phi_x)(l_3^2\phi_x+l_3m_3\phi_y+n_3l_3\phi_z)Sd\phi_1$$

$$+2k_{x_2}GA\int_{\theta_1}^{\theta_2}C_{ij}(2n_1n_2\phi_z+(m_1n_2+m_2n_1)\phi_y+(n_1l_2+n_2l_1)\phi_x)$$

$$(2l_1l_2\phi_x+(l_1m_2+l_2m_1)\phi_y+(n_2l_1+n_1l_2)\phi_z)Sd\phi_1$$

$$+2k_{y_2}GA\int_{\theta_1}^{\theta_2}C_{ij}(2n_2n_3\phi_z+(m_2n_3+m_3n_2)\phi_y+(n_2l_3+n_3l_2)\phi_x)$$

$$(2l_2l_3\phi_x+(l_2m_3+l_3m_2)\phi_y+(n_2l_3+n_3l_2)\phi_z)Sd\phi_1$$

$$+2GJ\int_{\theta_1}^{\theta_2}C_{ij}(2n_3n_1\phi_z+(m_3n_1+m_1n_3)\phi_y+(n_3l_1+n_1l_3)\phi_x)(2l_3l_1\phi_x+(l_3m_1+l_1m_3)\phi_y+(n_3l_1+n_1l_3)\phi_z)d\phi_1$$

In matrix :A_{22}

$$a_{ij}=2EI_{x_2}\int_{\theta_1}^{\theta_2}C_{ij}(m_1^2\phi_y+l_1m_1\phi_x+m_1n_1\phi_z)^2Sd\phi_1S+2EI_{y_2}\int_{\theta_1}^{\theta_2}C_{ij}(m_2^2\phi_y+l_2m_2\phi_x+m_2n_2\phi_z)^2Sd\phi_1$$

$$+2EA\int_{\theta_1}^{\theta_2}C_{ij}(m_3^2\phi_y+l_3m_3\phi_x+m_3n_3\phi_z)^2Sd\phi_1$$

$$+2k_{x_2}GA\int_{\theta_1}^{\theta_2}C_{ij}(2m_1m_2\phi_y+(l_1m_2+l_2m_1)\phi_x+(m_1n_2+m_2n_1)\phi_z)^2Sd\phi_1$$

$$+2k_{y_2}GA\int_{\theta_1}^{\theta_2}C_{ij}(2m_2m_3\phi_y+(l_2m_3+l_3m_2)\phi_x+(m_2n_3+m_3n_2)\phi_z)^2Sd\phi_1$$

$$+2GJ\int_{\theta_1}^{\theta_2}C_{ij}(2m_3m_1\phi_y+(l_3m_1+l_1m_3)\phi_x+(m_3n_1+m_1n_3)\phi_z)^2d\phi_1$$

In matrix A_{23}:

$$a_{ij}=2EI_{x_2}\int_{\theta_1}^{\theta_2}C_{ij}(n_1^2\phi_z+m_1n_1\phi_y+n_1l_1\phi_x)(m_1^2\phi_y+l_1m_1\phi_x+m_1n_1\phi_z)Sd\phi_1S$$

$$+2EI_{y_2}\int_{\theta_1}^{\theta_2}C_{ij}(n_2^2\phi_z+m_2n_2\phi_y+n_2l_2\phi_x)(m_2^2\phi_y+l_2m_2\phi_x+m_2n_2\phi_z)Sd\phi_1$$

$$+2EA\int_{\theta_1}^{\theta_2}C_{ij}(n_3^2\phi_z+m_3n_3\phi_y+n_3l_3\phi_x)(m_3^2\phi_y+l_3m_3\phi_x+m_3n_3\phi_z)Sd\phi_1$$

$$+2k_{x_2}GA\int_{\theta_1}^{\theta_2} C_{ij}(2n_1n_2\phi_z+(m_1n_2+m_2n_1)\phi_y+(n_2l_1+n_1l_2)\phi_x)$$

$$(2m_1m_2\phi_y+(l_1m_2+l_2m_1)\phi_x+(m_1n_2+m_2n_1)\phi_z)Sd\phi_1$$

$$+2k_{y_2}GA\int_{\theta_1}^{\theta_2} C_{ij}(2n_2n_3\phi_z+(m_2n_3+m_3n_2)\phi_y+(n_2l_3+n_3l_2)\phi_x)$$

$$(2m_2m_3\phi_y+(l_2m_3+l_3m_2)\phi_x+(m_2n_3+m_3n_2)\phi_z)Sd\phi_1$$

$$+2GJ\int_{\theta_1}^{\theta_2} C_{ij}(2n_3n_1\phi_z+(m_3n_1+m_1n_3)\phi_y+(n_3l_1+n_1l_3)\phi_x)$$

$$(2m_3m_1\phi_y+(l_3m_1+l_1m_3)\phi_x+(m_3n_1+m_1n_3)\phi_z)d\phi_1$$

In matrix A_{33}:

$$a_{ij}=2EI_{x_2}\int_{\theta_1}^{\theta_2} C_{ij}(n_1^2\phi_z+m_1n_1\phi_y+n_1l_1\phi_z)^2Sd\phi_1S+2EI_{y_2}\int_{\theta_1}^{\theta_2} C_{ij}(n_2^2\phi_z+m_2n_2\phi_y+n_2l_2\phi_x)^2Sd\phi_1$$

$$+2EA\int_{\theta_1}^{\theta_2} C_{ij}(n_3^2\phi_z+m_3n_3\phi_y+n_3l_3\phi_x)^2Sd\phi_1$$

$$+2k_{x_2}GA\int_{\theta_1}^{\theta_2} C_{ij}(2n_1n_2\phi_z+(m_1n_2+m_2n_1)\phi_y+(n_1l_2+n_2l_1)\phi_x)^2Sd\phi_1$$

$$+2k_{y_2}GA\int_{\theta_1}^{\theta_2} C_{ij}(2n_2n_3\phi_z+(m_2n_3+m_3n_2)\phi_y+(n_2l_3+n_3l_2)\phi_x)^2Sd\phi_1$$

$$+2GJ\int_{\theta_1}^{\theta_2} C_{ij}(2n_3n_1\phi_z+(m_3n_1+m_1n_3)\phi_y+(n_3l_1+n_1l_3)\phi_x)^2d\phi_1$$

$$A_{21}=A_{12},\ A_{31}=A_{13},\ A_{32}=A_{23},\ C_{ij}=\left(\frac{\pi}{\Delta\theta}\right)^2 i\cos\frac{i\pi(\phi_1-\theta_1)}{\Delta\theta}\ j\cos\frac{j\pi(\phi_1-\theta_1)}{\Delta\theta}$$

From Eq. (19), the coefficients a_i, b_i and c_i ($i=1$ to k) in the trial function (15) can be determined. Hence, the displacements of the stator tooth under the applied forces can be obtained.

4. Results and discussions

In order to obtain the displacement distribution within the stator tooth, the above equations have been implemented in a software tool developed in the Matlab environment. The parameters of the numerical example have been listed in Table 1. In operation of the drive, two magnetic forces are applied to one stator tooth. One force is applied along the radial direction of the planet and kept constant under the condition that the air-gap between the stator and planet teeth, and their material and size are determined. The force is perpendicular to the direction of the air-gap and has obvious effects on the air-gap. For the model machine developed by the authors, the load is about 10 N.

Table 1 Parameters of the example system

a/R	R (mm)	z_s	z_1	l (mm)	d (mm)	E (GPa)
2	30	20	8	12	6	210

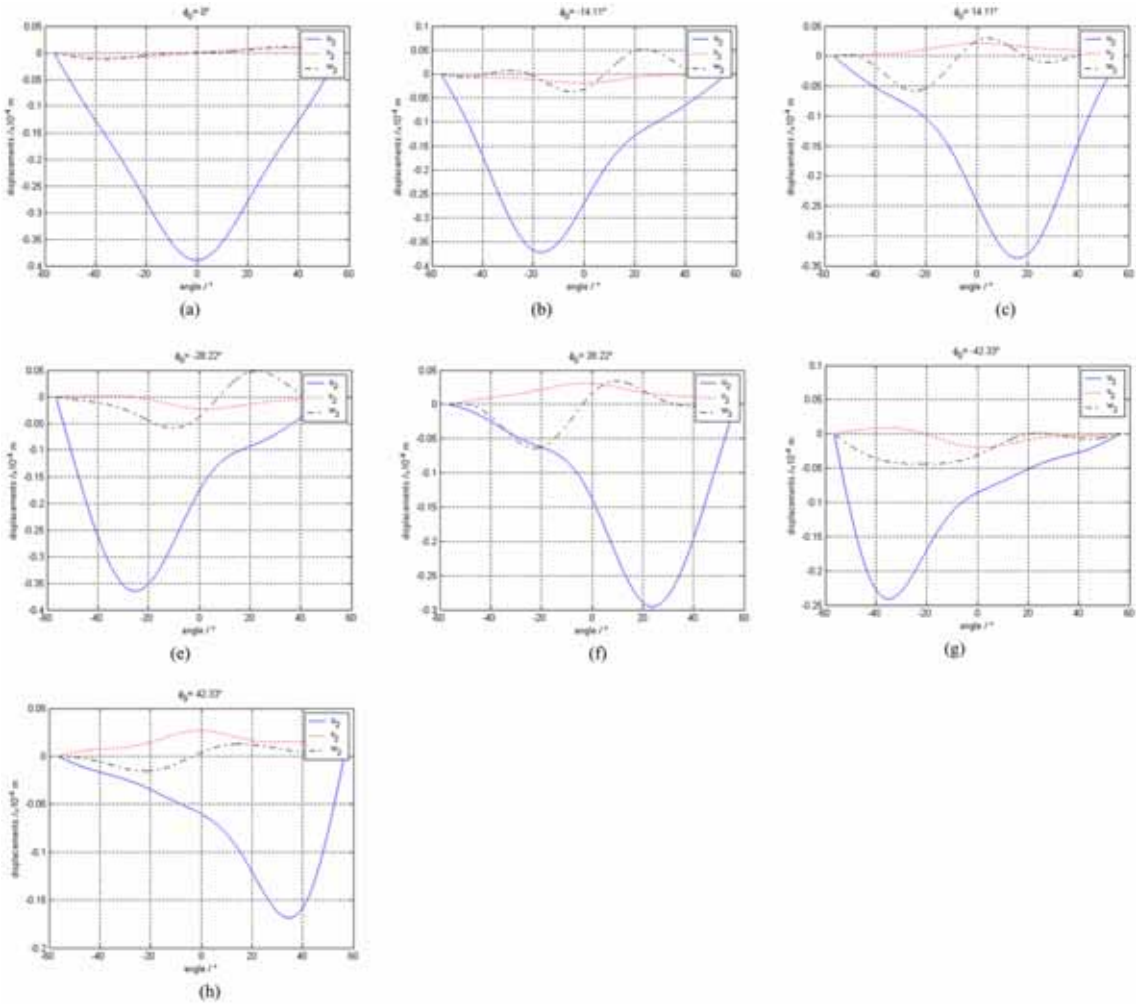

Fig. 4 The displacement distributions under load F_{bx2}

Hence, the force (load) is taken as 10 N in simulation. Another force is applied along the tangential direction of the planet tooth and its amplitude is dependent on the output torque. The force is parallel to the direction of the air-gap and has very small effects on the air-gap. Hence, the force (load) is also taken as 10 N in simulation. Fig. 4 shows the displacement distribution of the stator tooth under load F_{bx2} in the x_2 direction ($F_{bx2} = -10$ N $F_{by2} = 0$ N), Fig. 5 shows the displacement distribution of the stator tooth under load F_{by2} in the y_2 direction ($F_{bx2} = 0$ N $F_{by2} = 10$ N), Fig. 6 shows the displacement distribution of the stator tooth under loads F_{bx2} and F_{by2} ($F_{bx2} = -10$ N $F_{by2} = 10$ N).

From Figs. 4-6, one can observe the following facts:

(1) For the load applied to the stator tooth in the x_2 direction, the displacements u_2, v_2 and w_2 in three directions occur. The displacement u_2 in the x_2 direction is much larger than displacements v_2 and w_2 in the other two directions.

(2) As the mesh point between the planet and the stator changes, the maximum displacement in

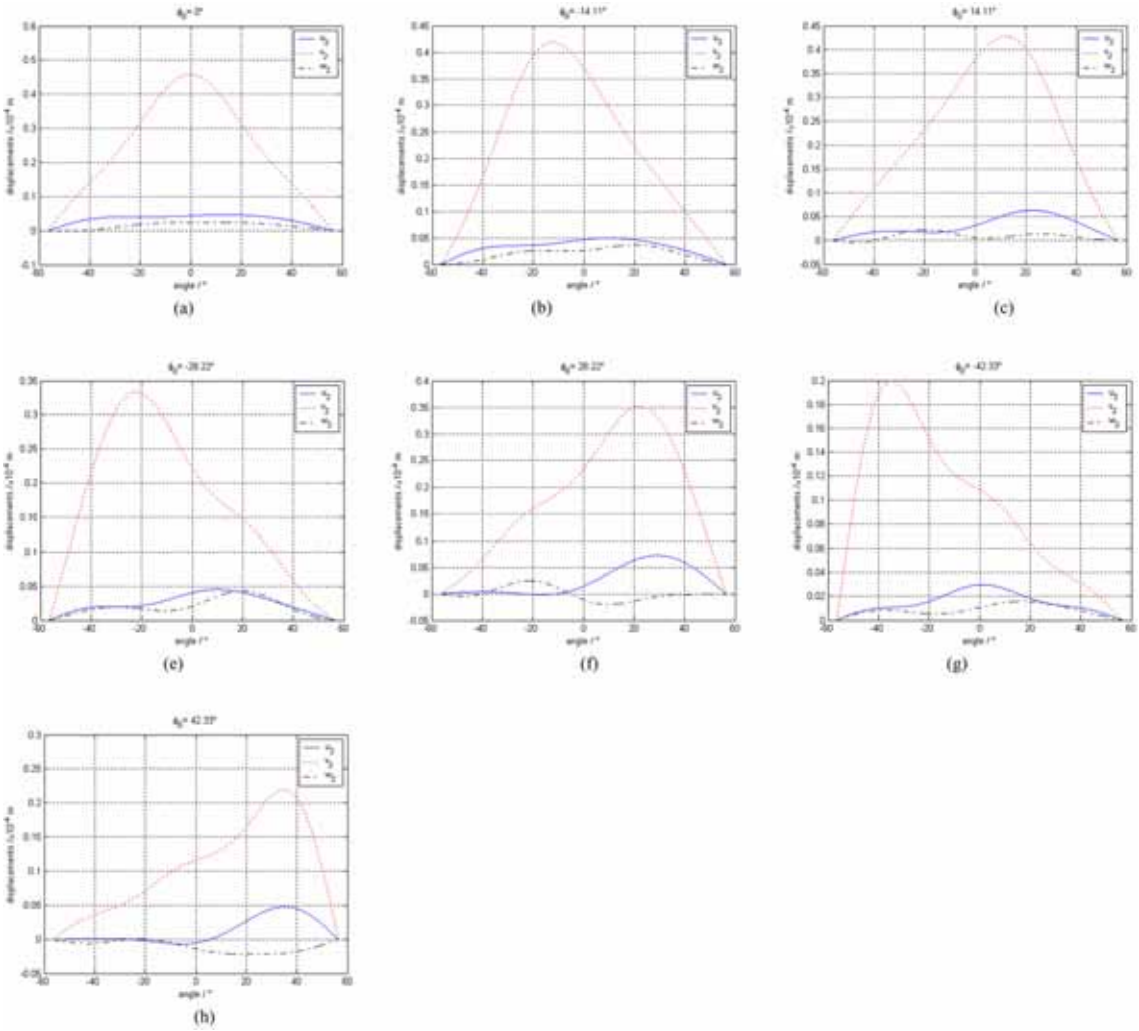

Fig. 5 The displacement distributions under load F_{by2}

the x_2 direction changes as well. When the mesh point is far from two ends of the stator tooth, the position of the maximum displacement $u_{2\max}$ is nearly identical to the mesh point. However, as the mesh point is near the two ends of the stator tooth, the shift between the position of the maximum displacement $u_{2\max}$ and the mesh point occurs. Such a position is located between the mesh point and the center point of the tooth, but it is near to the mesh point.

(3) When the two mesh points are symmetrical to the center point of the stator tooth, the displacement distributions are approximately symmetrical to the center point. However, they are not completely symmetrical, and the displacements for the mesh point in front of the center point of the stator tooth ($\phi_0 \le 0^0$) are a bit larger than those for the mesh point behind the center point of the stator tooth ($\phi_0 \ge 0^0$).

(4) As the stator tooth is spiral, displacement v_2 occurs in the y_2 direction when only the load in

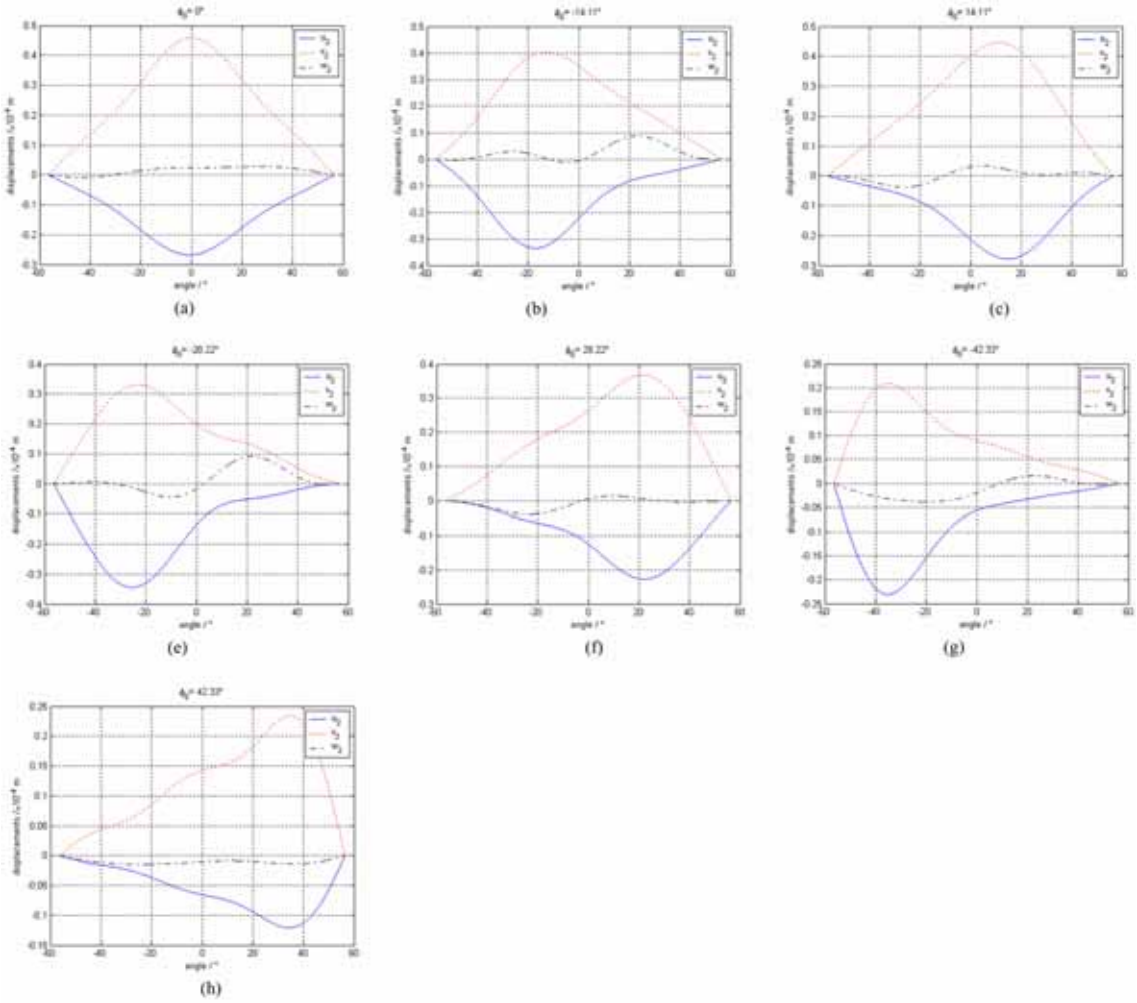

Fig. 6 The displacement distributions under loads F_{bx2} and F_{by2}

the x_2 direction is applied to the stator tooth.

(5) When the mesh point is in the center point of the stator tooth ($\phi_0 = 0^0$), the displacement v_2 is a minimum. When the mesh point moves toward the end point of the tooth, the displacement v_2 first grows then drops.

(6) When the mesh point is at center point of the tooth, the displacement v_2 is negative between the mesh point and one end point ($\varphi_0 \le 0^0$), and positive between the mesh point and another end point ($\varphi_0 \ge 0^0$).

(7) When the mesh point is within the angle range $\phi_0 \le 0^0$, the displacement v_2 is negative along the whole stator tooth, and when the mesh point is within the angle range $\phi_0 \ge 0^0$, the displacement v_2 is positive along the whole stator tooth.

(8) When only the load in the x_2 direction is applied to the stator tooth, the displacement w_2 occurs as well. The displacement w_2 is larger than the displacement v_2.

(9) When the mesh point is in the center point of the stator tooth ($\phi_0 = 0^0$), the displacement w_2

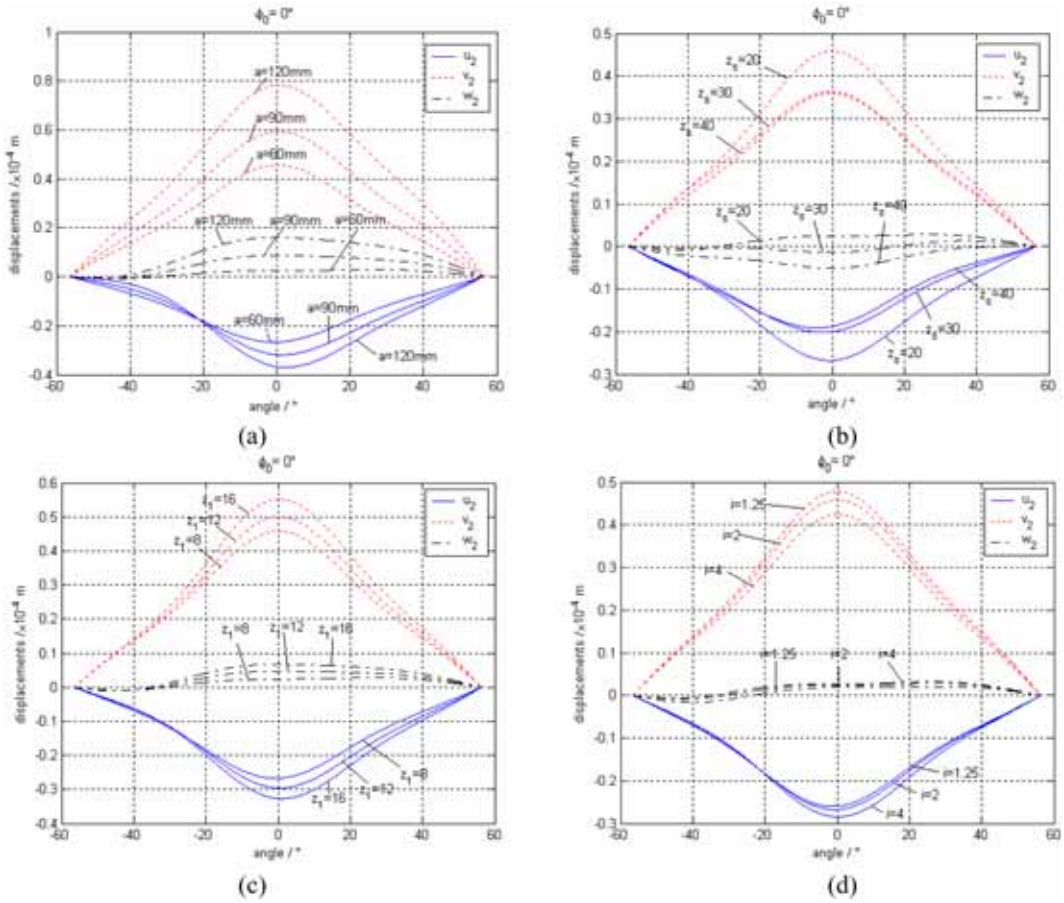

Fig. 7 Changes of the displacement distributions along with the main parameters

is also a minimum. When the mesh point moves toward the end point of the tooth, the displacement w_2 first grows then drops as well.

(10) Along the whole stator tooth, tensile stain zone ($w_2 \geq 0$) and compression strain zone ($w_2 \leq 0$) occur. At most mesh points, one tensile stain zone and one compression strain zone occur. At some mesh points, two tensile stain zones or two compression stain zones occur.

(11) When only the load in the y_2 direction is applied to the stator tooth, the displacements u_2, v_2 and w_2 in three directions occur as well. The displacement v_2 in the y_2 direction is much larger than displacements u_2 and w_2 in the other two directions.

(12) As the mesh point between the planet and the stator changes, the maximum displacement in the y_2 direction changes as well. The changes are similar to those of the displacement u_2 mentioned above.

(13) When the two mesh points are symmetrical to the center point of the stator tooth, the displacement v_2 distributions are approximately symmetrical to the center point as well. However, the displacements for the mesh point behind the center point of the stator tooth ($\phi_0 \geq 0^0$) are a bit larger than those for the mesh point in front of the center point of the stator tooth ($\phi_0 \leq 0^0$).

(14) As the stator tooth is spiral, displacement u_2 occurs in the x_2 direction when only the load in the y_2 direction is applied to the stator tooth.
(15) When the mesh point is in the center point of the stator tooth ($\phi_0 = 0^0$), the displacement u_2 is a minimum as well. When the mesh point moves toward the end point of the tooth, the displacement u_2 first grows then drops.
(16) When only the load in the y_2 direction is applied to the stator tooth, the displacement w_2 occurs as well. The displacement w_2 is smaller than the displacement u_2. The changes of displacement w_2 here are similar to the case when only the load in the x_2 direction is applied to the stator tooth.
(17) When the loads in the x_2 and y_2 directions are applied to the stator tooth simultaneously, the displacements u_2, v_2 and w_2 in three directions occur as well. However, both u_2 and v_2 are large.
(18) Under the condition that the load in the x_2 direction is equal to the load in the y_2 direction, the displacement in the y_2 direction is larger than that in the x_2 direction.
(19) When the loads in the x_2 and y_2 directions are applied to the stator tooth simultaneously, the displacement w_2 is also larger than the case when only the load in one direction is applied.
(20) Along the whole tooth, the displacements u_2 are all negative and the displacements v_2 are all positive for any mesh points.

Fig. 7 shows the variation of the displacement distributions versus the main parameters. Here, the mesh point is at $\phi_0 = 0^0$, $F_{bx2} = -10N$ and $F_{by2} = 10N$, i is the ratio of the length to width of the section of the stator tooth, $i = l/d$. From Fig. 7, the following observations can be made:

(1) For constant planet radius R, as the center distance a increases, the displacements u_2, v_2 and w_2 grow, among which the increase of the displacement v_2 is more obvious. For constant planet radius R, as the center distance a increases, the lead angle of the stator tooth becomes small and the length of the stator tooth increases, so the displacements grow with increasing center distance.
(2) As the stator tooth number z_s increases, the displacements u_2 and v_2 drop. When the stator tooth number is small, the decrease of the displacements along with tooth number z_s is obvious. When the stator tooth number is large, the decrease of the displacements along with tooth number z_s is very small. As the stator tooth number z_s increases, the lead angle of the stator tooth becomes large and the length of the stator tooth decreases, so the displacements drop with increasing tooth number z_s. When the tooth number z_s is large, the length variation of the stator tooth along with the tooth number z_s is quite small, so the decrease of the displacements along with the tooth number z_s is not obvious.
(3) As the stator tooth number z_s increases, the displacement w_2 first drops then grow in the opposite direction.
(4) As the planet tooth number z_1 increases, the displacements u_2, v_2 and w_2 grows. It is also because the lead angle of the stator tooth becomes small and the length of the stator tooth increases with increasing the planet tooth number.
(5) As the ratio i increases, the displacements u_2 and w_2 grows, but v_2 drops.
(6) These results show that the related parameters have obvious influence on the displacement distribution of the stator tooth. In order to decrease the displacements of the stator tooth, these parameters should be selected properly.

Here, a FEM analysis package, ANSYS, is used to simulate the elastic displacements of the stator tooth (see Fig. 8). The differences between the FEM results and those by the strain energy method are compared in Table 2. The results show that the maximum error of the displacements is smaller than 15%, which illustrates the applicability of the results presented in the paper.

Table 2 The comparison of the maximum displacements from FEM and energy method

	Energy method (m)	FEM (m)	errors
u	0.0000275	0.0000236	14.18%
v	0.0000315	0.0000268	14.92%
w	0.0000330	0.0000305	4.55%

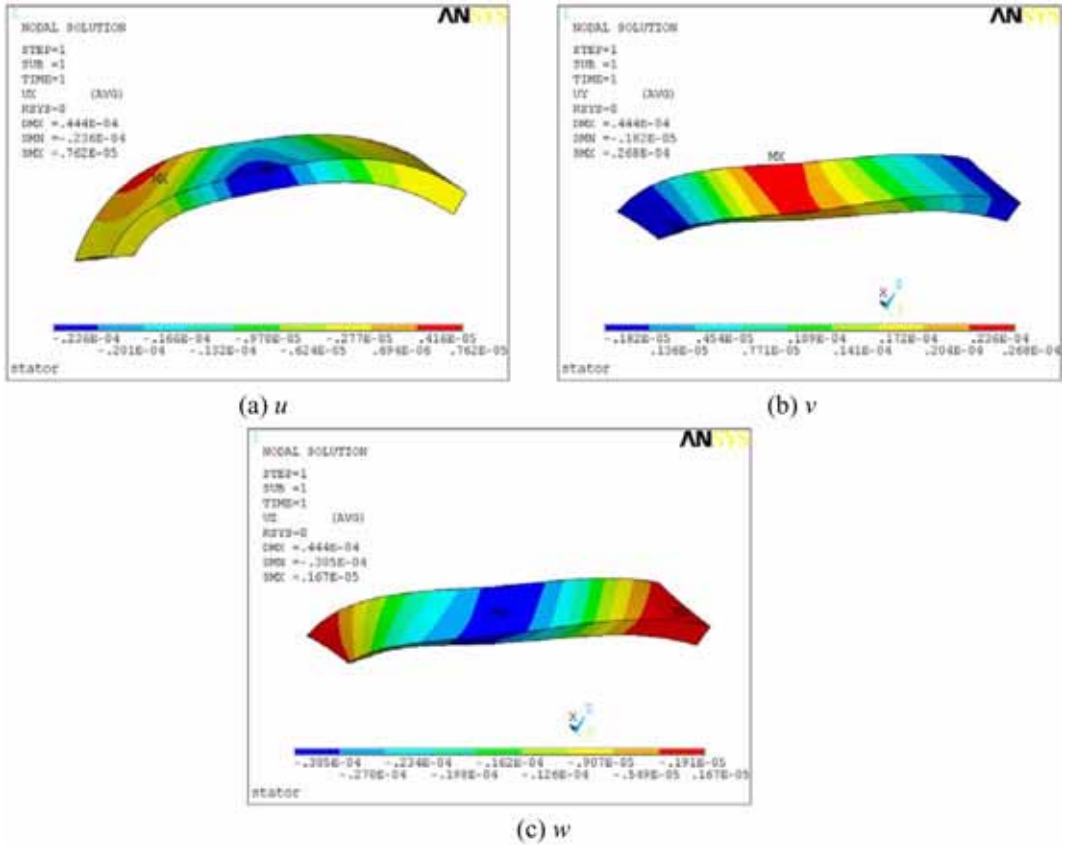

Fig. 8 The elastic displacements of the stator tooth from FEM

5. Conclusions

In this paper, we use the coordinate transformation method and express the displacements of the stator tooth in the local coordinate system as a function of the variables in the drive coordinate system. By the minimum potential energy principle, the equations of the displacements of the stator tooth under the loads are derived. The displacement distributions within the stator tooth for the drive system are investigated. The results show that the related parameters have obvious influence on the displacement distribution of the stator tooth. In order to decrease the displacements of the stator tooth, these parameters should be properly selected.

Acknowledgments

The results presented in this paper were carried out through a research project supported by National Natural Science Foundation of China (No50375132).

References

Kuehnle, M.R., Peeken, H., Troeder, H. and Cerniak, S. (1981), "The Toroidal drive", *Mech. Eng*., **103**(2), 32-39.

Yao, L., Dai, J.S. and Wei, G. (2006), "Characteristics with respect to different meshing rollers of the toroidal drive", *Mech. Mach. Theory*, **41**(7), 863-881.

Wei, G., Yao, L., Cai, Y. and Dai, J.S. (2008), "Latency errors in the mathematical modelling and meshing characteristics of the toroidal drive", *Math. Comput. Model.*, **47**(9-10), 827-854.

Mezani, S., Atallah, K. and Howe, D. (2006), "A high-performance axial-field magnetic gear", *J. Appl. Phys.*, **99**(8), 1-3(08R303).

Jorgensen, F.T., Andersen, T.O. and Rasmussen, P.O. (2008), "The cycloid permanent magnetic gear", *IEEE T. Ind. Appl.*, **44**(6), 1659-1665.

Wang, J., Mezani, S. and David, H. (2006), "A novel high-performance linear magnetic gear", *IEEE T. Ind. Appl*., **126**(10), 1352-1356.

Liu, X., Chau, K.T., Jiang, J.Z. and Yu, C.(2009), "Design and analysis of interior-magnet outer-rotor concentric magnetic gears", *J. Appl. Phys.*, **105**(7), 1-3(07F101).

Delin, Z. and Huamin, L. (1993), "Side surface harmonic stepper motor", *J. Mech. Eng.(in China)*, **29**(5), 96-98.

Oliver, B. (2000), "Harmonic piezodrive-miniaturized servo motor", *Mechatronics*., **10**(4), 545-554.

Xu, L. and Huang, Z. (2003), "Contact Stresses for Toroidal drive", *J. Mech. Design*, **125**(3),165-168.

Xu, L. and Huang, J. (2005), "Torque for Electromechanical Integrating Toroidal drive", *P. I. Mech. Eng. C-J Mec.*, **219**(8), 801-811.

Xu, L. and Fan, S. (2006), "Design and torque control for electromechanical integrating toroidal drive", *Mech. Mach. Theory*, **41**(2), 230-245.